Bull Earthquake Eng (2017) 15:4319–4347
DOI 10.1007/s10518-017-0141-7

ORIGINAL RESEARCH PAPER

Development of wood and steel diaphragm hysteretic connector database for performance-based earthquake engineering

Maria Koliou[1] · **Andre Filiatrault**[2,3]

Received: 28 September 2016 / Accepted: 20 April 2017 / Published online: 27 April 2017

Abstract Performance-based earthquake engineering (PBEE) considers certain metrics to assess the seismic response of buildings, which integrate economic losses into the design process. PBEE requires the development and use of reliable nonlinear response analysis models to simulate the seismic performance of structures through collapse. The structural damage is assessed by evaluating physical damage caused by engineering demand parameters (EDPs), while the nonlinear numerical models are used to conduct dynamic analyses for varying levels of seismic intensity to compute the values of the representative EDPs. Accurate representation of structural members' stiffness and strength deterioration (hysteretic) parameters plays an important role into simulating dynamic response through collapse. These parameters' values are usually calibrated to a large number of experimental data. The development of a hysteretic parameter database for wood and steel diaphragm connectors is presented in this paper. The wood diaphragm connectors are commonly used in light-frame wood building construction for shear walls or roof diaphragms. The steel diaphragm connectors are used for building structures that incorporate steel frame roof diaphragms. The experimental data were used for quantifying the hysteretic parameters of two well-known nonlinear models considered into structural modeling as well as evaluating their energy dissipation properties. Case studies on the collapse performance assessment of a light-frame wood wall system and a low-rise building incorporating a steel roof system were conducted to demonstrate the usefulness of the diaphragm connector database.

✉ Maria Koliou
Maria.Koliou@colostate.edu

[1] Department of Civil and Environmental Engineering, Center of Excellence for Risk-Based Community Resilience Planning, Colorado State University, 1372 Campus Delivery, Engineering Building, Fort Collins, CO 80523, USA

[2] Department of Civil, Structural and Environmental Engineering, State University of New York at Buffalo, Buffalo, NY 14260, USA

[3] School of Advanced Studies IUSS Pavia, 27100 Pavia, Italy

Keywords Diaphragm connectors · Steel roof · Wood diaphragms · Collapse assessment · Energy dissipation properties · Performance-based earthquake engineering

1 Introduction

The next-generation performance-based earthquake engineering (PBEE) framework (Cornell and Krawinkler 2000; Moehle and Deierlein 2004; Porter 2003) was developed by the Pacific Earthquake Engineering Research (PEER) Center to evaluate the earthquake-induced risk of structures based on specified performance metrics and objectives. Performance objectives are commonly expressed as the probability of exceeding a certain damage state, varying between linear elastic response to complete collapse, for a given seismic intensity. The PBEE framework is comprised of four main steps including hazard characterization, structural and damage analysis, and loss assessment. In the first step of the PBEE framework, a ground motion intensity (intensity measure—IM) is selected and through probabilistic seismic hazard analysis, the mean annual rate of exceedance of the ground motion IM for a specified site and characteristics of the structure, uncertainties in earthquake size, and distances to the faults is generated. The most common seismic IMs are the spectral acceleration and displacement at the fundamental period of the structure. In the second step of the framework, nonlinear simulation models are developed to describe the response of the structure subjected to a set of earthquake ground motions scaled to the selected IM. The results of the nonlinear analyses define the engineering demand parameters (EDPs) of the structure under study. Story drift ratios, shear forces, floor absolute accelerations and overturning moments are the most commonly used EDPs for building structures (Lignos and Krawinkler 2012), whereas displacement ductility, peak absolute acceleration and normalized hysteretic energy dissipated are EDPs often used for bridge structures (Conte and Zhang 2007). The EDPs then relate to damage measures (DMs) in the third step of the PBEE framework, which explicitly describe the damage to structural and non-structural components. In the final step of the framework, the DMs are considered to assess the decision variables (DVs), such as the replacement cost, downtime and loss of life, through probabilistic loss models.

Accurate nonlinear numerical models able to simulate the response of the structure are essential to generate representative metrics for the EDPs used in the PBEE framework. The damage levels associated with EDPs are highly dependable on: (1) amplification of drift demands due to second order P-Δ effects, and (2) strength and stiffness deterioration of the structural components, which contribute to the structural collapse. In order to accurately capture the cyclic deterioration of structural components, several hysteretic models have been developed for steel (Ibarra et al. 2005; Jin and El-Tawil 2003; Krishnan 2010; Uriz et al. 2008), reinforced concrete (Baber and Noori 1985; Barham et al. 2005; Neuenhofer and Filippou 1998; Otani 1981; Sideris and Salehi 2016; Sivaselvan and Reinhorn 2000, 2006) and wood (Ceccotti and Vignioli 1990; Christovasilis 2011; Dolan 1989; Folz and Filiatrault 2001; Kivell et al. 1981; Stewart 1987) components the last three decades. In order to model accurately structural collapse, the deterioration parameters of these various models need to be predicted. These parameters' values are usually calibrated using a large number of experimental data. Therefore, the development of hysteretic component databases is essential for this calibration process. Databases on structural components

including statistical information of various properties of structural components are available in the literature for reinforced concrete (Berry et al. 2004; Lignos and Krawinkler 2012) and steel (Lignos et al. 2012, 2013; Lignos and Krawinkler 2012) members, i.e. beams, columns and connections.

The main objective of this paper is to develop a hysteretic parameter database for wood and steel diaphragm connectors and illustrate its usefulness for accurate nonlinear modeling through collapse. Robust nonlinear modeling of wood shear walls or steel roof diaphragms includes explicit consideration of each individual sheathing panel and fastener (e.g. nails, screws etc.) as well as shear and bending deformations of sheathing and framing members (Bahmani and van de Lindt 2014; Christovasilis 2010; Koliou 2014; Koliou et al. 2017a; Tremblay and Rogers 2005). Therefore, it is of great significance to have access to a wide database of connectors/fasteners to account for the variability in the parameters used in nonlinear modeling. The database includes statistical parameters for two well-known hysteretic models for several types of wood and steel diaphragm connectors including common nails, welds, button punches, power actuated fasteners and pins based on a large number of experimental data available in the literature. Furthermore, information on the energy dissipation properties of each connector type is provided for possible consideration in Direct Displacement-Based Design (DDBD). In order to demonstrate the utilization and importance of the diaphragm connector database for predicting collapse performance in the context of PBEE, two case studies are presented in this paper: one on a light-frame wood wall system and another one on a low-rise building with a steel roof diaphragm.

2 Nonlinear modeling

Two hysteretic models, Wayne-Stewart (Stewart 1987) and CUREE-SAWS (Folz and Filiatrault 2001), are used in this study to develop the hysteretic connector database. Both hysteretic models were developed for light-frame wood elements, however they are used in this study to capture the hysteretic response of steel diaphragm connectors as well. The Wayne-Stewart hysteretic model, shown in Fig. 1a, has a tri-linear envelope (backbone) curve that allows strength degradation, while it also displays pinching and stiffness degradation. The CUREE-SAWS model is a parametric hysteretic model incorporating exponential loading curves, unloading stiffness degradation, and variation of force-

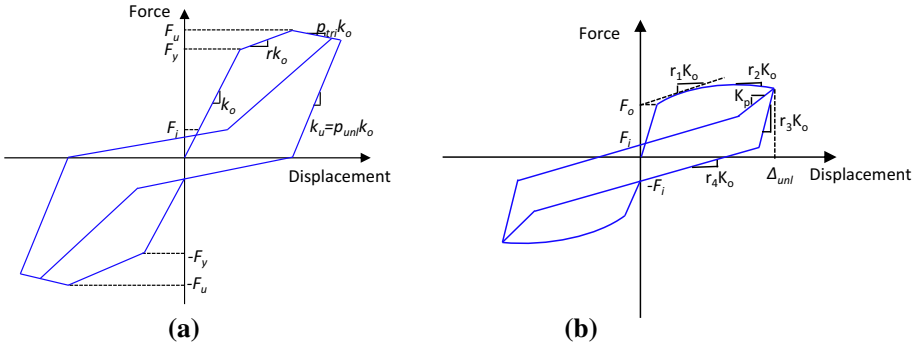

Fig. 1 Hysteretic response of: **a** Wayne-Stewart model (data from Stewart 1987) and **b** CUREE-SAWS model (data from Folz and Filiatrault 2001)

intercept at zero displacement as well as degraded backbone for strength degradation (see Fig. 1b). Both hysteretic models are incorporated into several nonlinear analysis software (e.g. OpenSees, RUAUMOKO, CASHEW, SAPWood, Timber3D). The hysteretic parameters developed in this study can be used for modeling diaphragms elements within these software platforms. The hysteretic parameters describing both hysteretic models are summarized in Table 1.

For the purpose of this study, MATLAB codes (MATLAB 2013) were generated for both hysteretic models considering simplified uniaxial plasticity concepts. For example, for the Wayne-Stewart model, four yielding surfaces were considered. Two of these surfaces were fixed and two moving/updated based on the previous history of the response. This simplified uniaxial plasticity modeling concept using multiple yielding surfaces is graphically illustrated for the Wayne-Stewart model in Fig. 2.

3 Hysteretic connector database for performance-based earthquake engineering

The hysteretic database was developed for wood and steel diaphragm framing connectors. The load–displacement data considered for the database development were available in the public literature through reports and journal publications. The connector database includes the following information:

- Metadata: Configuration, geometry, testing details and loading conditions.
- Reported experimental results including digitized load–displacement hysteretic curves.
- Optimized hysteretic parameters (and their statistics) for Wayne-Stewart and CUREE-SAWS hysteretic models to be used for modeling of diaphragm components.
- Comparison plots between test results and fitted analytical response using the optimized hysteretic parameters, as well as energy absorption comparison plots.
- Information on the energy dissipation properties of each connector type for further consideration in Direct-Displacement Based Design (DDBD) of structures whose response is highly dependable to diaphragm connectors.

Table 1 Summary of parameters describing Wayne-Stewart and CUREE-SAWS hysteretic models

Wayne-Stewart	CUREE-SAWS
Initial yield force (F_y)	Intercept strength for the asymptotic line to the envelope curve (F_o)
Linear elastic stiffness (k_o)	Linear elastic stiffness (k_o)
Secondary stiffness factor (r)	Secondary stiffness factor (r_1)
Trilinear factor beyond ultimate force (p_{tri})	Degradation stiffness factor (r_2)
Unloading stiffness factor (p_{unl})	Unloading stiffness factor (r_3)
Ultimate force (F_u)	Pinching stiffness factor (r_4)
Intercept force (F_i)	Intercept force (F_i)
–	Unloading displacement (Δ_{unl})
–	Stiffness degradation parameter (a)
–	Strength degradation parameter (β)

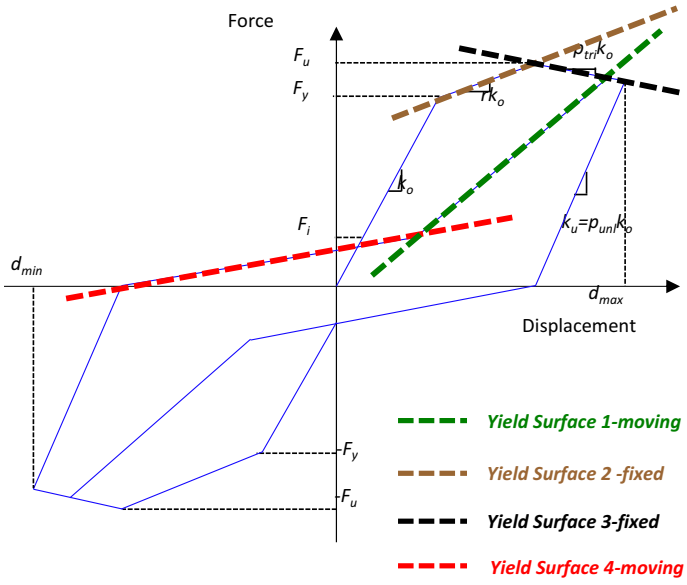

Fig. 2 Simplified uniaxial plasticity modeling of the Wayne-Stewart model using multiple yielding surfaces

To optimize the hysteretic parameters associated with the two hysteretic models (Wayne-Stewart and CUREE-SAWS), a set of MATLAB (MATLAB 2013) codes was developed. The optimal hysteretic parameters were computed through an identification process to match numerical and experimental data of each connector test by minimizing the differences in force and deformation. The identification process was set as a constrained nonlinear least squares problem described by:

$$\min_{\vec{x}}\left(\left\|\vec{f}\left(\vec{x}\right)\right\|_2\right)^2 \quad s.t. \quad \vec{x}_{lb} \le \vec{x} \le \vec{x}_{ub} \tag{1}$$

where $\vec{f}\left(\vec{x}\right)$ is the error function defined by Eq. (2), $\vec{x}_{lb}$ is a lower bound vector of all model parameters and $\vec{x}_{ub}$ is an upper bound vector of all parameters

$$f(\vec{x}, i) = F_{test}(i) - F_{estim}(i) \tag{2}$$

where $F_{test}(i)$ is the force of each connector test at a given time step i, $F_{estim}(i)$ is the force estimated for either the Wayne-Stewart or the CUREE-SAWS hysteretic models at a given time step i for the optimized/fitted hysteretic properties values of vector $\vec{x}$.

A starting point vector for all the hysteretic parameters associated with both hysteretic models (Wayne-Stewart and CUREE-SAWS), and lower and upper bound vectors of these parameters were defined to be used for the estimation of the force and deformation of each connector test at each time step. The initial upper and lower bound vectors of the hysteretic properties of the Wayne-Stewart and CUREE-SAWS models were defined based on a trial and error basis. The robust Trust Region Reflective (TRR) algorithm was used to solve the least square minimization problem (Yuan 2000). Analysis convergence was satisfied in this study for a specified tolerance equal to 10^{-5}. Examples of satisfactory calibrations of both wood and steel diaphragm connectors are shown in Fig. 3.

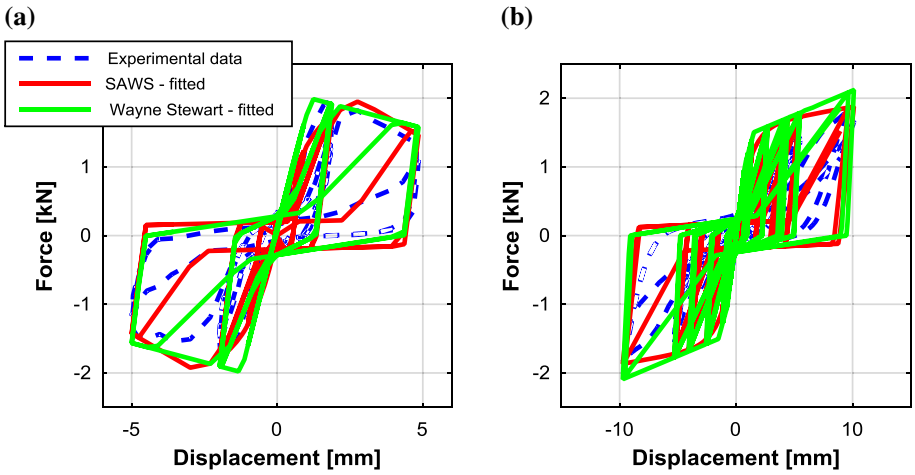

Fig. 3 Examples of calibration of hysteretic parameters of Wayne-Stewart and CUREE-SAWS models to simulate the hysteretic response of: **a** 10d common nails (data from Coyne 2007) and **b** framing welds (data from Rogers and Tremblay 2003b)

The uncertainty/variability of the statistical parameters (median and standard deviation) values for the different hysteretic properties can considerably affect the accuracy of the performance indicators (e.g. EDPs). The number of experimental test repetitions, loading protocols and conditions are some of the parameters that can affect the uncertainty introduced in the statistical values of the connector model hysteretic properties. Such uncertainties may lead to an under- or over-estimation of collapse capacity of the structural system studied. However, the sensitivity of the hysteretic parameters of wood and steel connectors are out of the scope of this study.

3.1 Wood connector database

Extensive experimental studies on the response of wood diaphragm-to-framing connectors have been conducted during the last five decades and are summarized in Table 2. The most recent and representative cyclic test programs on diaphragm connectors conducted by Fonseca and Campbell (2002), Christovasilis et al. (2009), and Coyne (2007) were considered for creating the connector database.

Fonseca and Campbell (2002) performed extensive experiments on wood framing-to-sheathing connectors connections under cyclic loading to be incorporated into the CUREE-SAWS computer program. The main variables of the test program and configuration were: type and thickness of sheathing panel, type of wood member [i.e. Douglas Fir-Larch (DF-L) and Pressure-Treated Hem-Fir (PT HF)], moisture conditions at assembling and testing time, type and size of fastener, edge distance, overdriven depth and direction of loading. Two types of sheathing panels were considered for this investigation including oriented strand board (OSB) and plywood, while four different thicknesses of 9.5 mm (3/8 in.), 11.1 mm (7/16 in.), 11.9 mm (15/32 in.) and 15.1 mm (19/32 in.) were tested. The type of fasteners used for the testing included nails, wood screws and staples of different geometries. All specimens were tested both parallel and longitudinal to the grain of the wood member.

Table 2 Summary of experimental investigations on wood diaphragm connectors

Investigator/source	Type of loading	Study objectives
Mack (1961, 1962)	Monotonic and cyclic	Repetitive loading effects
Leach (1964)	Monotonic	Effect of moisture on nailed connectors' strength and stiffness
Wilkinson (1976)	Cyclic	Nailed and bolted timber connector's response under vibrational loading
Soltis and Mtenga (1985)	Monotonic and cyclic	Dynamic response of nailed connections at frequencies of 1 and 10 Hz
Dowrick (1986)	Cyclic	Hysteretic response of nailed and bolted timber connectors
Chou (1987)	Cyclic	Nonlinear load-slip relation and non-viscous damping in wood joints
Dean et al. (1989)	Cyclic	Hysteretic response of timber connectors and indicated the presence of initial slackness during dynamic loading
Ni (1997)	Monotonic and cyclic	Effect of loading regimes on hysteretic response of nailed connectors
Mohammad (1997)	Monotonic	Effects of multi-phase moisture conditioning on nailed connectors' stiffness
Dolan et al. (1995)	Monotonic and cyclic	Effects of cyclic loading on the performance and safety of nailed and bolted connectors
Fonseca and Campbell (2002)	Monotonic and cyclic	Establish a parameter database for sheathing-to-wood connectors
Christovasilis et al. (2009)	Monotonic and cyclic	Determine hysteretic properties of connectors to be implemented in analytical models
Coyne (2007)	Monotonic and cyclic	Determine hysteretic properties of wood deck connectors
Huang (2013)	Monotonic	Determine properties of connection analytical model for specific type of nail fasteners

Christovasilis et al. (2009) performed wood framing-to-sheathing connection tests similar to those by Fonseca and Campbell (2002) to determine the hysteresis properties of the nail connectors used for a full scale wood townhouse tested at the University at Buffalo (Filiatrault et al. 2009). Thirteen configurations were tested varying the loading direction on the framing (parallel and perpendicular) relative to the grain as well as the framing properties (Hem Fir) including 50.8 mm × 101.6 mm (2 × 4) and 50.8 mm × 152.4 mm (2 × 6). Oriented strand board (OSB) and 8d common nails of 63.5 mm (2.5 in.) length and 3.38 mm (0.13 in.) diameter were considered for all tests conducted (Christovasilis et al. 2009).

Finally, Coyne (2007) conducted experimental studies on representative wood framing-to-sheathing connections to determine their hysteresis properties. The test program included both monotonic and cyclic test protocols. Different combinations of sheathing [i.e. 11.11 mm (7/16 in.), 15.88 mm (5/8 in.) and 19.05 mm (3/4 in.)] and nails (6d, 8d and 10d common nails) were connected to 50.8 mm × 101.6 mm (2 × 4) Hem Fir wood framing.

A summary of the wood diaphragm connector types, specimen configurations and test repetitions considered for developing the wood diagram connector database is presented in Table 3. The hysteretic parameters of both the Wayne-Stewart and the CUREE-SAWS

models were fitted to match with high level of accuracy the experimental test data, as described earlier in this paper. The statistical parameters (median and standard deviation) for each hysteretic parameter of corresponding wood diaphragm connector were generated and are listed in Tables 4 and 5 for Wayne Stewart and CUREE-SAWS hysteretic models, respectively. Comparison plots between experimental and numerical/fitted hysteretic responses for W-1 [6d common nails, 50.8 mm × 101.6 mm (2 × 4) Hem Fir wood framing and 11.11 mm (7/16 in.) OSB] and W-6 [10d common nails, 50.8 mm × 101.6 mm (2 × 4) Hem Fir wood framing and 15.88 mm (5/8 in.) OSB] connectors along with their energy absorbed histories are also presented in Figs. 4 and 5, respectively. Comparison plots for all wood diaphragm connectors can be found in Koliou (2014).

The parameters of both hysteretic models summarized in the wood connector database can be used for nonlinear modeling of wood diaphragm components such as roof and wall systems.

Table 3 Summary of wood diaphragm connector characteristics considered in developing the database

Database ID	Connector type	Connector characteristics	Specimen characteristics[a]	Number of specimen tested	Source
W-1	6d common nails	d = 2.87 mm (0.113 in.) l = 50.8 mm (2.0 in.)	2 × 4 Hem Fir 7/16 OSB std.	10	Coyne (2007)
W-2	8d common nails	d = 2.87 mm (0.113 in.) l = 63.5 mm (2.5 in.)	2 × 4 Hem Fir. and 7/16 OSB std.	19	Christovasilis et al. (2009)
W-3			2 × 6 Hem Fir. and 7/16 OSB std.	17	
W-4		d = 3.33 mm (0.131 in.) l = 63.5 mm (2.5 in.)	2 × 4 Hem Fir and 7/16 OSB std.	10	Coyne (2007)
W-5	10d common nails	d = 3.76 mm (0.148 in.) l = 76.2 mm (3 in.)	2 × 4 Hem Fir 7/16 and OSB std.	11	Coyne (2007)
W-6			2 × 4 Hem Fir and 5/8 OSB std.	10	
W-7			2 × 4 Hem Fir and 3/4 OSB std.	9	
W-8	10d box nails	d = 3.33 mm (0.131 in.) l = 76.2 mm (3 in.)	DF-L and 19/32 T&G	20	Fonseca and Campbell (2002)
W-9			DF-L & 19/32 OSB std.	20	
W-10	#10 Rolled–Hardened screws	d = 2.87 mm (0.113 in.) l = 50.8 mm (2.0 in.)	DF-L & 7/16 OSB std.	20	Fonseca and Campbell (2002)

d diameter, *l* length

[a] in. inches

Table 4 Fitted parameters and dispersion characteristics of wood diaphragm connectors for Wayne-Stewart hysteretic model

Database ID	Statistical parameter	F_y, N (lbs)	k_o, kN/m (lbs/in)	r	p_{tri}	p_{unl}	F_u, N (lbs)	F_i, N (lbs)
W-1	Median	887.0 (199.4)	272.8 (1557.6)	0.171	−0.076	2.058	1247.7 (280.5)	161.0 (36.2)
	SD	175.3 (39.4)	16.9 (96.4)	0.080	0.059	0.540	10.7 (2.4)	1.8 (0.4)
W-2	Median	939.9 (211.3)	655.7 (3744.1)	0.331	−0.137	2.595	1099.6 (247.2)	218.4 (49.1)
	SD	243.3 (54.7)	126.5 (722.2)	0.097	0.073	0.857	18.2 (4.1)	4.9 (1.1)
W-3	Median	955.9 (214.9)	479.9 (2740.4)	0.369	−0.095	1.854	1359.4 (305.6)	197.1 (44.3)
	SD	532.5 (119.7)	11.4 (64.8)	0.137	0.036	0.563	49.2 (11.2)	12.9 (2.9)
W-4	Median	927.0 (208.4)	385.0 (2198.6)	0.417	−0.044	2.026	1374.1 (308.9)	204.2 (45.9)
	SD	278.9 (62.7)	33.4 (190.9)	0.183	0.012	0.681	20.9 (4.7)	3.1 (0.7)
W-5	Median	930.6 (209.2)	407.1 (2324.4)	0.689	−0.032	2.448	1452.8 (326.6)	218.9 (48.3)
	SD	241.5 (54.3)	30.8 (175.8)	0.121	0.006	0.911	21.8 (4.9)	3.6 (0.8)
W-6	Median	1488.8 (334.7)	343.0 (1958.5)	0.582	−0.072	2.671	1634.7 (367.5)	222.9 (50.1)
	SD	242.0 (54.4)	26.2 (149.7)	0.139	0.054	1.008	20.5 (4.6)	4.5 (1.00)
W-7	Median	1607.1 (361.3)	650.5 (3714.4)	0.268	−0.105	2.138	1936.3 (435.3)	303.8 (68.3)
	SD	242.0 (54.4)	64.2 (366.5)	0.120	0.053	0.194	9.8 (2.2)	3.6 (0.8)
W-8	Median	726.8 (163.4)	505.8 (2888.3)	0.419	−3.824	3.254	1376.3 (309.4)	183.3 (41.2)
	SD	197.9 (44.5)	68.5 (390.9)	0.176	2.046	0.962	16.9 (3.8)	6.7 (1.5)
W-9	Median	829.2 (186.4)	376.5 (2149.9)	0.469	−1.767	2.916	1478.1 (332.2)	188.2 (42.3)
	SD	310.5 (69.8)	95.0 (542.4)	0.170	1.003	1.229	31.6 (7.1)	7.1 (1.6)
W-10	Median	1278.0 (287.3)	284.6 (1625.3)	0.589	−2.012	3.207	2080.9 (467.8)	290.9 (65.4)
	SD	272.2 (61.2)	32.9 (188.2)	0.132	1.467	1.217	23.1 (5.2)	11.1 (2.5)

Table 5 Fitted parameters and dispersion characteristics of wood diaphragm connectors for CUREE-SAWS hysteretic model

Database ID	Statistical parameter	F_o, N (lbs)	k_o, kN/m (lbs/in)	r_1	r_2	r_3	r_4	F_i, N (lbs)	Δ_{unl}, mm (in.)	α	β
W-1	Median	845.2 (190.0)	378.0 (2158.6)	0.020	−0.039	1.022	0.005	104.5 (23.5)	9.4 (0.369)	0.77	1.01
	SD	193.1 (43.4)	28.3 (161.3)	0.007	0.007	0.053	0.004	34.3 (7.7)	0.7 (0.028)	0.05	0.21
W-2	Median	967.5 (217.5)	948.2 (5414.5)	0.020	−0.044	1.031	0.005	178.8 (40.2)	13.2 (0.521)	0.73	1.17
	SD	114.3 (25.7)	402.5 (2298.4)	0.023	0.014	0.005	0.002	20.9 (4.7)	1.0 (0.040)	0.00	0.04
W-3	Median	940.8 (211.5)	691.6 (3949.3)	0.020	−0.038	1.021	0.008	102.8 (23.1)	14.3 (0.563)	0.74	1.37
	SD	320.7 (72.1)	145.0 (828.1)	0.025	0.016	0.140	0.001	47.2 (10.6)	2.8 (0.111)	0.05	0.22
W-4	Median	903.0 (203.0)	1030.8 (5886.0)	0.020	−0.027	1.016	0.010	91.6 (20.6)	9.0 (0.355)	0.79	1.04
	SD	81.4 (18.3)	409.3 (2337.1)	0.028	0.022	0.002	0.002	12.0 (2.7)	0.5 (0.020)	0.00	0.04
W-5	Median	923.0 (207.5)	1174.6 (6707.3)	0.020	−0.021	1.024	0.005	94.3 (21.2)	7.9 (0.312)	0.77	1.12
	SD	126.8 (28.5)	279.4 (1595.3)	0.006	0.014	0.295	0.001	33.8 (7.6)	1.3 (0.052)	0.20	0.30
W-6	Median	1431.9 (321.9)	1035.7 (5914.0)	0.020	−0.036	1.029	0.005	104.5 (23.5)	12.0 (0.471)	0.73	1.04
	SD	101.9 (22.9)	258.1 (1473.7)	0.004	0.010	0.001	0.001	16.9 (3.8)	1.8 (0.070)	0.00	0.00
W-7	Median	1654.3 (371.9)	1171.7 (6690.7)	0.020	−0.054	1.019	0.005	143.2 (32.2)	10.9 (0.429)	0.72	1.41
	SD	405.2 (91.1)	43.3 (247.3)	0.007	0.010	0.328	0.002	78.7 (17.7)	2.6 (0.104)	0.22	0.35
W-8	Median	740.2 (166.4)	825.1 (4711.5)	0.020	−0.039	1.011	0.005	84.5 (19.0)	9.0 (0.353)	0.71	1.36
	SD	84.5 (19.0)	161.4 (921.7)	0.001	0.019	0.306	0.001	2.2 (0.5)	1.0 (0.041)	0.05	0.25
W-9	Median	839.8 (188.8)	976.0 (5573.2)	0.020	−0.039	1.015	0.005	93.9 (21.1)	8.6 (0.339)	0.73	1.08
	SD	105.9 (23.8)	147.6 (843.0)	0.012	0.015	0.237	0.001	14.7 (3.3)	1.7 (0.066)	0.08	0.29
W-10	Median	1105.8 (248.6)	248.6 (1419.3)	0.020	−0.039	1.019	0.005	111.65 (25.1)	6.1 (0.239)	0.89	1.86
	SD	624.5 (140.4)	153.0 (873.5)	0.004	0.026	0.048	0.005	67.6 (15.2)	3.7 (0.147)	0.13	0.27

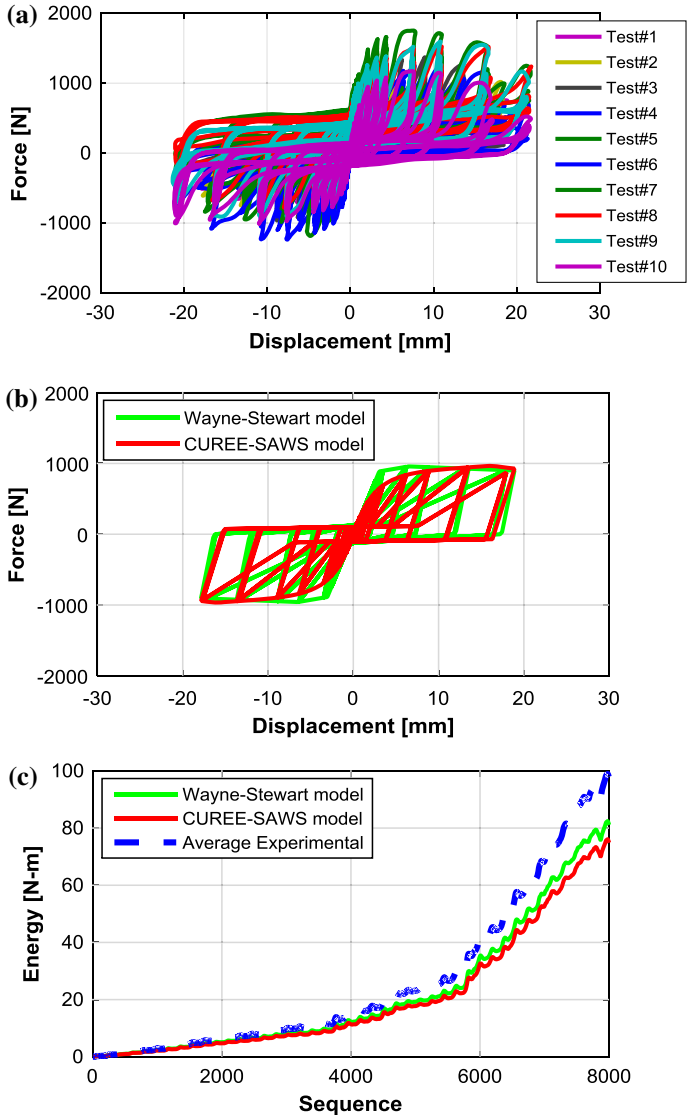

Fig. 4 Hysteretic response of 6d common nails (W-1): **a** experimental results, **b** fitted–optimal hysteretic models and **c** energy absorption

3.2 Steel connector database

Several experimental studies on the response of steel diaphragm cold form connectors under monotonic loading have been conducted, as summarized in Table 6. These studies

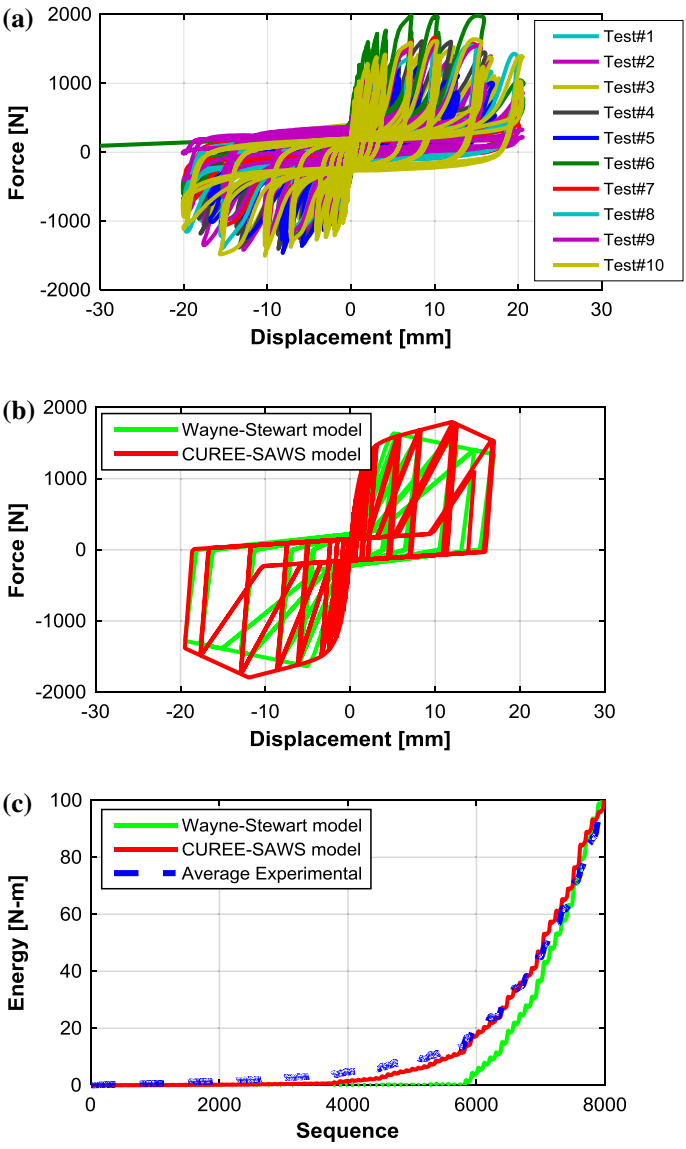

Fig. 5 Hysteretic response of 10d common nails (W-6): **a** experimental results, **b** fitted–optimal hysteretic models and **c** energy absorption

included mainly testing of welded and screwed connectors. Contrary to wood diaphragm connectors, limited test data is available in the public literature on the cyclic response of steel diaphragm connectors. The most recent studies on this type of connectors under cyclic loading which are limited to research conducted in Canada for specific types of connections, are considered in the development of the steel diaphragm connector database.

Rogers and Tremblay (2003a, b) tested steel diaphragm connectors, in order to investigate the inelastic seismic response of connections for low rise buildings incorporating

Table 6 Summary of experimental investigations on steel diaphragm connectors

Investigator/source	Type of loading	Study objectives
Yarnell and Pekoz (1973)	Monotonic	Investigate the performance of welded puddle (arc-spot) and fillet welded connections (122 specimens tested)
Pekoz and McGuire (1980)	Monotonic	Investigate the response of arc-spot welds and revise the welding provisions at the time (342 tests conducted)
Pekoz (1990)	N/A	Summarize 3500 screwed connection tests conducted in US, Canada, Sweden and the Netherlands to formulate screw connection design provisions
Zadanfarrokh and Bryan (1992)	Monotonic	Analysis and testing of bolted connections. Test results used to formulate design expressions
LaBoube and Yu (1993)	Monotonic	Evaluate the tensile strength of arc spot welds and formulate design guidelines (260 tests conducted)
Walter (1995)	Monotonic and cyclic	Investigate the performance of powder actuated bolts, screws, rivets and welds under low cycle fatigue
Sokol et al. (1998)	Monotonic	Establish test protocol/method for determining the strength of screwed connections (uniaxial tension, shear and combined shear and tension tests conducted)
LaBoube and Sokol (2002)	Monotonic	Investigate the behavior of self-drilling screwed connections in residential construction. Several parameters of interest on connections' strength were studied (fastener patterns, screw spacing, stripped screws and number of screws)
Peuler et al. (2002)	Monotonic and cyclic	Examine the inelastic response of arc-spot welded deck-to-frame connections. Different test configurations considered: with and without washers, various steel deck thicknesses and different electrode types (235 specimens tested)
Rogers and Tremblay (2003a, b)	Monotonic and cyclic	Investigate the inelastic response of steel connections for steel low rise buildings. Tests on screwed, nailed, powder-actuated fasteners, welded, button punched and welded connections conducted
Fülöp and Dubina (2006)	Monotonic	Study the performance of self-drilling screws under quasi-static as well as high velocity loading. Framing connections of steel panels as well as seam connections (very thin steel panels) were tested
Snow (2008)	Monotonic	Determine relationship between arc spot weld shear strength and the arc time used to form the weld
Guenfoud (2009)	Monotonic and cyclic	Establish welding process to produce quality welds if multiple layers of sheet steel are connected to framing members. Examine the applicability of design protocols for arc spot welds

metal deck roof systems. A series of experiments on screwed, nailed, powder-actuated fasteners, welded, and button punched (see Fig. 6) connections were conducted under monotonic, cyclic, quasi-static and earthquake motion shear tests. It was observed that the ultimate capacity as well as the energy dissipation differed for the several connection types. The powder-actuated fasteners (PAFs) exhibited the highest energy dissipation, followed by the screwed and nailed connections. The welded connections developed significant ultimate capacities; however, they failed at small displacements resulting in low energy dissipation. Button punched exhibited slippage at low load, while welded connections developed higher resistance and remained attached up to large displacements amplitudes.

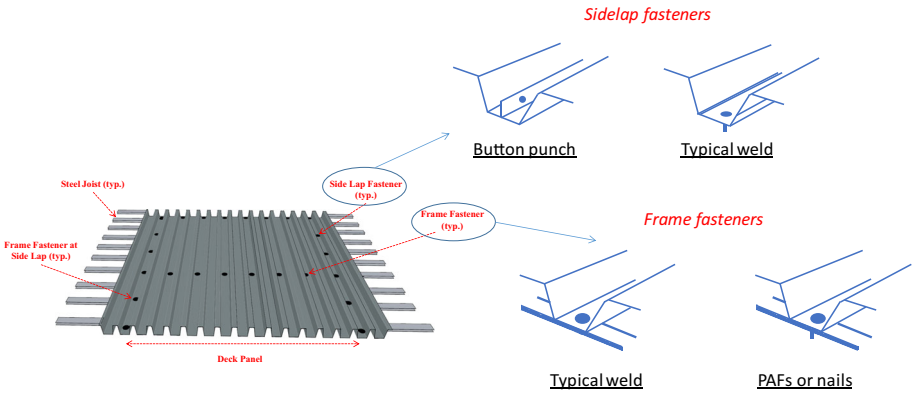

Fig. 6 Examples of typical steel roof diaphragm connectors

Guenfoud (2009) investigated the tensile and shear capacity of arc spot welded connections for multiple layers of sheet steel connected to framing members. The main objectives of this study were to establish a quality welding process and examine the applicability of design protocols for arc spot welds. The study reported that the most crucial parameters during the welding process of thick steel sheathing panels are the current setting, the electrode type and the welding technique. More than one hundred specimens of different steel sheet thicknesses and welding procedures were tested under monotonic and cyclic loading. The experimental results were compared to the current (at the time) Canadian provisions to verify the applicability of multi-overlap configurations.

The experimental results from Guenfoud (2009), Rogers and Tremblay (2003a, b) were considered in this study for the development of the steel diaphragm hysteretic connector database, as summarized in Table 7. Similar to the wood diaphragm connector database, the statistical parameters for each hysteretic parameter and corresponding steel diaphragm connector were generated and are summarized in Tables 8 and 9 for Wayne Stewart and CUREE-SAWS hysteretic models, respectively. Furthermore, plots comparing the experimental and numerical/fitted hysteretic responses for S-2 (button punches) and S-9 (PAFs) connectors and their energy absorbed histories are illustrated in Figs. 7 and 8, respectively. All steel diaphragm connectors comparison plots can be found in Koliou (2014).

3.3 Evaluation of diaphragm connector energy dissipation properties

The seismic response of structural diaphragm elements (i.e. walls, roofs) is directly dependent on the performance of their connectors, which is strongly related to their ability to dissipate energy. The equivalent viscous damping ratio is a common measure used to evaluate energy dissipation capacity. It was computed herein for each type of connector included in the database. The fitted parameters of the CUREE-SAWS hysteretic model were considered for each type of connector to evaluate the equivalent viscous damping ratio as a function of the displacement amplitude achieved in each cycle. Only the CUREE-SAWS hysteretic model was considered since it is a smooth exponential hysteretic model compared to the tri-linear Wayne-Stewart model.

The equivalent viscous damping, ξ_{eq}, was calculated as (e.g. Chopra 2006):

Table 7 Summary of steel diaphragm connector characteristics considered in developing the database

Database ID	Connector type	Connector characteristics	Specimen characteristics	Number of specimen tested	Source
S-1	Button punch	Diameter = 9.9 mm (0.39 in.)	22 ga deck	2	Rogers and Tremblay (2003a)
S-2			20 ga deck	2	
S-3	Screws	Dimensions = 254–355.6 × 22.2 mm (10–14 × 7/8 in.)	22 ga deck	2	
S-4			20 ga deck	2	
S-5	Welds	Length = 35.05 mm (1.38 in.)	22 ga deck	2	
S-6	Powder-actuated fasteners	(Hilti EDNK22-THO12 & Buildex BX12)	22 ga deck to 3.05 mm (0.12 in.) plate	4	Rogers and Tremblay (2003b)
S-7			20 ga deck to 3.05 mm (0.12 in.) plate	4	
S-8	Powder-actuated fasteners	(Hilti ENPH2-21-L15 & Buildex BX14)	22 ga deck to 20.1 mm (0.79 in.) plate	4	
S-9			20 ga deck to 20.1 mm (0.79 in.) plate	4	
S-10	Buildex screws	Dimensions = 304.8–355.6 × 25.4 mm (12–14 × 1 in.)	22 ga deck to 3.05 mm (0.12 in.) plate	2	
S-11			20 ga deck to 3.05 mm (0.12 in.) plate	2	
S-12	Hilti screws	Dimensions = 304.8–609.6 × 22.2 mm (12–24 × 7/8 in.)	22 ga deck to 3.05 mm (0.12 in.) plate	2	
S-13			20 ga deck to 3.05 mm (0.12 in.) plate	2	
S-14	Welds and washer	16 mm (0.63 in.) arc spot	22 ga deck to 3.05 mm (0.12 in.) plate	1	
S-15			22 ga deck to 3.05 mm (0.12 in.) plate	2	
S-16	Welds	16 mm (0.63 in.) arc spot	22 ga deck to 20.1 mm (0.79 in.) plate	1	
S-17			20 ga deck to 3.05 mm (0.12 in.) plate	2	
S-18	Welds	16–19.05 mm (0.63–0.75 in.) arc spot	2 ply–16 ga deck to 6.35 mm (0.25 in.) plate	4	Guenfoud (2009)
S-19			2 ply–18 ga deck to 6.35 mm (0.25 in.) plate	4	
S-20			2 ply–20 ga deck to 6.35 mm (0.25 in.) plate	4	
S-21			2 ply–22 ga deck to 6.35 mm (0.25 in.) plate	4	
S-22			4 ply–16 ga deck to 6.35 mm (0.25 in.) plate	4	
S-23			4 ply–18 ga deck to 6.35 mm (0.25 in.) plate	3	
S-24			4 ply–20 ga deck to 6.35 mm (0.25 in.) plate	4	
S-25			4 ply–22 ga deck to 0.25 in. plate	4	

$$\xi_{eq} = \frac{E_{D,\Delta_{\max}}}{2\pi k_{eq}\Delta_{\max}^2} \quad (3)$$

where $E_{D,\Delta max}$ is the energy dissipated at a given cycle of displacement amplitude $\Delta_{\max}$, and k_{eq} is the corresponding secant stiffness.

The equivalent viscous damping was computed at all displacement amplitudes considering the first two loading cycles. Basic characteristic of the CUREE-SAWS hysteretic model is that after the second loading cycle at the same displacement amplitude, the hysteretic response remains constant. Therefore, the damping characteristics of the second cycle may be used for analysis and design purposes. The variations of the equivalent viscous damping ratio with displacement amplitudes for the different types of connectors, as presented in Figs. 9 and 10, for wood and steel diaphragm connectors, respectively, indicate that the damping ratio varies between 10 and 15% of critical for all common nails, button punches, screws and welds. Higher damping ratios were obtained for powder actuated fasteners varying between 25 and 30% of critical. The fact that the damping ratio for different connections is approximately the same for several connector types could be beneficial in Direct-Displacement Based Design (DDBD) of building structures incorporating wood and/or steel diaphragm systems by simplifying the design methodology.

4 Case studies: collapse assessment using database information for diaphragm connectors

Two case studies were considered in this paper to demonstrate the utilization of the diaphragm connector database for both wood and steel connectors including strength and stiffness deterioration in the numerical modeling for predicting the collapse capacity of buildings and building components. The response of a light-frame wood wall system and a low-rise building incorporating a steel roof diaphragm were investigated through collapse analyses.

4.1 Light-frame wood wall system

The utilization of the wood diaphragm connector database for collapse performance assessment of building components is illustrated through a case study of a light-frame wood shear wall tested by Bahmani and van de Lindt (2014) under cyclic loading. The 2.4 m × 2.4 m (8 ft × 8 ft) wood structural panels tested were sheathed with 11.9 mm (15/32 in.) plywood attached with 8d common nails to the framing. The 8d common nails were placed at 102 mm (4 in.) and 305 mm (12 in.) on center (o.c.) for edge and field nail spacing, respectively. The sheathing material was attached to 2 × 4 Douglas-fir-larch (DFL) framing with studs at 406 mm (16 in.) o.c. The wall specimen were designed to represent the old (archaic) material and boundary conditions used in 1940–1960 buildings located in San Francisco Bay Area. Site visits and inspections were conducted to gather data regarding the material, wall configurations and boundary conditions (Bahmani 2016). A modified CUREE loading protocol with a loading rate 0.1 Hz instead of 0.2 Hz was used to perform the cyclic tests.

The numerical and experimental response of the wood frame wall system under cyclic loading was compared to evaluate the accuracy for the numerical model considered for the collapse studies.

Table 8 Fitted parameters and dispersion characteristics of steel diaphragm connectors for Wayne-Stewart hysteretic model

Database ID	Statistical parameter	F_y, N (lbs)	k_o, kN/m (lbs/in)	r	p_{tri}	p_{unl}	F_u, N (lbs)	F_i, N (lbs)
S-1	Median	1814.0 (407.8)	1496.7 (8546.2)	0.852	−0.086	2.057	2762.8 (621.1)	199.3 (44.8)
	SD	320.3 (72.0)	132.4 (756.2)	0.111	0.058	1.289	10.7 (2.4)	14.2 (3.2)
S-2	Median	1440.3 (323.8)	2046.6 (11,686.6)	0.340	−0.074	2.013	2431.0 (546.5)	776.2 (174.5)
	SD	888.3 (199.7)	102.1 (582.8)	0.198	0.043	0.928	54.7 (12.3)	35.1 (7.9)
S-3	Median	4671.5 (1050.2)	2861.1 (16,337.3)	0.365	−0.120	2.015	5321.4 (1196.3)	490.2 (110.2)
	SD	360.3 (81.0)	25.9 (147.9)	0.091	0.008	0.208	12.0 (2.7)	2.7 (0.6)
S-4	Median	3306.4 (743.3)	2711.9 (15,485.4)	0.366	−0.410	2.912	3904.2 (877.7)	330.9 (74.4)
	SD	604.1 (135.8)	21.0 (119.7)	0.189	0.051	0.176	18.2 (4.1)	0.0 (0.007)
S-5	Median	4253.4 (956.2)	10,511.6 (60,022.9)	0.203	−0.025	1.651	4800.1 (1079.1)	112.1 (25.2)
	SD	460.8 (103.6)	1151.9 (6577.3)	0.004	0.006	0.086	18.2 (4.1)	71.6 (16.1)
S-6	Median	3706.7 (833.3)	9166.0 (52,339.4)	0.336	−0.016	2.963	4510.1 (1013.9)	196.6 (44.2)
	SD	531.6 (119.5)	344.7 (1968.4)	0.192	0.001	1.842	153.0 (34.4)	105.0 (23.6)
S-7	Median	4279.2 (962.0)	7427.7 (42,413.4)	0.214	−0.017	2.353	5081.6 (1142.4)	83.2 (18.7)
	SD	705.5 (158.6)	563.8 (3219.3)	0.002	0.004	0.375	168.6 (37.9)	73.8 (16.6)
S-8	Median	3699.6 (831.7)	10,392.4 (59,342.3)	0.201	−0.017	2.092	4773.4 (1073.1)	122.8 (27.6)
	SD	230.9 (51.9)	1197.1 (6835.6)	0.001	0.002	0.159	63.6 (14.3)	58.7 (13.2)
S-9	Median	5603.9 (1259.8)	5100.7 (29,125.9)	0.223	−0.012	4.096	6028.7 (1355.3)	120.1 (27.0)
	SD	403.0 (90.6)	1733.1 (9896.3)	0.054	0.074	0.651	13.8 (3.1)	65.8 (14.8)
S-10	Median	4544.7 (1021.7)	4000.0 (22,840.8)	0.331	−0.022	3.399	4858.3 (1092.2)	531.6 (119.5)
	SD	196.6 (44.2)	575.4 (3285.5)	0.078	0.015	0.793	13.8 (3.1)	22.2 (5.0)
S-11	Median	7922.3 (1781.0)	5873.5 (33,538.6)	0.232	−0.061	2.558	5489.1 (1234.0)	494.6 (111.2)
	SD	468.0 (105.2)	883.0 (5041.9)	0.051	0.054	1.196	28.0 (6.3)	52.9 (11.9)
S-12	Median	5968.6 (1341.8)	13,491.1 (77,035.9)	0.230	−0.017	1.718	6390.8 (1436.7)	816.7 (183.6)
	SD	379.4 (85.3)	298.8 (1706.1)	0.135	0.008	0.164	38.7 (8.7)	46.7 (10.5)
S-13	Median	5094.1 (1145.2)	1952.4 (11,148.4)	0.676	−0.057	1.854	6516.6 (1465.0)	2214.3 (497.8)
	SD	1399.0 (314.5)	1211.0 (6915.2)	0.019	0.049	0.314	552.5 (124.2)	190.4 (42.8)

Table 8 continued

Database ID	Statistical parameter	F_y, N (lbs)	k_o, kN/m (lbs/in)	r	p_{tri}	p_{unl}	F_u, N (lbs)	F_i, N (lbs)
S-14	Median	8811.0 (1980.8)	25,220.2 (144,011.2)	0.201	−0.068	3.111	13,338.0 (2998.5)	2151.2 (483.6)
	SD	N/A[a]	N/A[a]	N/A[a]	N/A[a]	N/A[a]	N/A[a]	N/A[a]
S-15	Median	7896.0 (1775.1)	25,131.4 (143,504.0)	0.201	−0.294	2.321	12,820.7 (2882.2)	2527.9 (568.3)
	SD	442.6 (99.5)	365.5 (2087.0)	0.001	0.216	0.342	1462.1 (328.7)	383.9 (86.3)
S-16	Median	8604.6 (1934.4)	32,959.5 (188,203.7)	0.275	−0.282	2.333	14,116.9 (3173.6)	1049.8 (236.0)
	SD	N/A[a]	N/A[a]	N/A[a]	N/A[a]	N/A[a]	N/A[a]	N/A[a]
S-17	Median	9992.5 (2246.4)	46,282.9 (264,282.3)	0.210	−0.067	4.053	15,269.9 (3432.8)	3662.7 (823.4)
	SD	1243.3 (279.5)	9331.8 (53,286.1)	0.006	0.055	1.902	723.7 (162.7)	24.0 (5.4)
S-18	Median	19,042.4 (4280.9)	35,367.2 (201,952.0)	0.200	−0.048	3.635	19,503.7 (4384.6)	6545.1 (1471.4)
	SD	2471.4 (555.6)	224.6 (1282.6)	0.002	0.039	3.103	186.8 (42.0)	346.5 (77.9)
S-19	Median	11,947.9 (2686.0)	24,791.3 (141,561.7)	0.202	−0.091	5.550	12,528.9 (2816.6)	5419.3 (1218.3)
	SD	2349.6 (528.2)	749.8 (4281.5)	0.103	0.071	2.047	122.3 (27.5)	355.4 (79.9)
S-20	Median	6491.7 (1459.4)	18,920.7 (108,039.9)	0.201	−0.031	4.359	6687.9 (1503.5)	3006.1 (675.8)
	SD	351.4 (79.0)	287.5 (1641.9)	0.004	0.013	1.618	8.5 (1.9)	12.5 (2.8)
S-21	Median	8188.3 (1840.8)	4502.4 (25,709.5)	0.256	−0.109	7.403	8802.6 (1978.9)	687.7 (154.6)
	SD	986.6 (221.8)	202.8 (1158.0)	0.067	0.022	3.630	32.5 (7.3)	77.4 (17.4)
S-22	Median	10,410.6 (2340.4)	18,630.3 (106,381.8)	0.219	−0.144	1.852	11,191.7 (2516.0)	624.5 (140.4)
	SD	1048.9 (235.8)	645.1 (3683.5)	0.071	0.036	0.978	52.9 (11.9)	70.7 (15.9)
S-23	Median	6447.3 (1449.4)	19,111.5 (109,129.6)	0.200	−0.093	2.872	7607.8 (1710.3)	1393.2 (313.2)
	SD	755.8 (169.9)	19.2 (109.9)	0.046	0.026	1.146	0.2 (0.05)	800.7 (180.0)
S-24	Median	9060.6 (2036.9)	39,635.1 (226,322.2)	0.232	−0.258	8.308	9896.4 (2224.8)	209.5 (47.1)
	SD	578.3 (130.0)	46.9 (267.8)	0.089	0.137	1.126	222.9 (50.1)	31.6 (7.1)
S-25	Median	12,415.4 (2791.1)	16,241.6 (92,742.1)	0.215	−0.035	3.871	12,746.8 (2865.6)	5014.5 (1127.3)
	SD	2080.9 (467.8)	533.6 (3047.1)	0.123	0.008	2.542	287.8 (64.7)	383.0 (86.1)

[a] Limited data sample to compute standard deviation

A wall frame model was developed in the SAPWood software (Pei and van de Lindt 2010) to address the wall configuration experimentally investigated. The wood shear wall was modeled following the geometric configuration of the test set up as well as the nailing schedule incorporated. The CUREE-SAWS hysteretic model was used to model the 8d common nails. The shear wall was modeled with 8d common nails with diameter of 3.33 mm, length equal to 63.5 mm and 11 mm (7/16 in.) thick oriented strand board (OSB) sheathing, whose hysteretic properties were obtained by the wood diaphragm connector database (W-4). The displacement-based CUREE protocol followed during the experimental investigation by Bahmani and van de Lindt (2014) was considered to conduct cyclic analysis of the wood frame wall model. The numerical and experimental cyclic responses of the wood shear wall are compared in Fig. 11. It is observed that the numerical wall model captures with very good accuracy the experimental force–deformation response.

The wall model was further used in this study to conduct nonlinear time history analyses for increasing seismic intensities—incremental dynamic analyses (IDAs) (Vamvatsikos and Cornell 2002)—under the FEMA P695 (FEMA 2009) Far-Field ground motion ensemble. The total seismic weight considered in the analyses of the wood wall system was calculated equal to the wall dead load of 0.26 kPa (5.5 psf) accounting for the weight of the framing member (2 × 4 DFL at 400 mm) and the sheathing material [11.9 mm (15/32 in.) plywood]. Assuming that the wall system is a typical first story exterior wall of a two-story residential building, the gravity load was assumed to be applied to the wall. The footprint of the conventional light-frame wood residential building was assumed equal to 8.5 m × 13.4 m (28 ft × 44 ft). The wall gravity load was computed accounting for the roof, wall and floor dead load equal to 4.93 kN/m (338 plf).

Collapse fragility curves as a function of the spectral acceleration (S_a) at the fundamental period of the wall system were developed and presented in Fig. 12 for a damping ratio of 5% of critical. The collapse fragilities were conditioned on a collapse limit state defined by the last survival intensity before the numerical building model becomes unstable for the light-frame wood wall system. The drift ratio was the EDP considered in this case study. A lognormal distribution is fitted considering the Maximum Likelihood Estimation (MLE) (Baker 2015) to the collapse fragility function with a median capacity of 1.59 g and a logarithmic standard deviation of 0.40. The hysteretic properties of the wood diaphragm connectors are an essential part of the modeling process that is necessary for computing the median collapse capacity accurately.

4.2 Low-rise building incorporating steel roof

A second case study was conducted and presented herein to demonstrate the utilization of the steel diaphragm connector database. A low-rise industrial building incorporating a flexible steel roof was considered to perform collapse response analyses. The building structure investigated is of a footprint of 30.48 m × 30.48 m (100 ft × 100 ft) and consists of concrete tilt-up wall panels (vertical elements of seismic force resisting system—SFRS) and steel roof diaphragm (horizontal elements of SFRS). The wall panels were designed to be 7.62 m (25 ft) wide and 9.14 m (30 ft) tall incorporating a 0.91 m (3 ft) tall parapet. The 22 ga steel roof diaphragm was detailed with Hilti X-ENDK22-THQ12 PAFs and #10 screws at 457.2 mm (18″) o.c. for framing and sidelap connectors, respectively. Their hysteretic properties were obtained by the steel diaphragm connector database S-6 and S-3, for the framing and sidelap connectors, respectively. A fastener pattern of 36/9 was considered for the design of the roof diaphragm. The low-rise industrial building was

Table 9 Fitted parameters and dispersion characteristics of steel diaphragm connectors for CUREE-SAWS hysteretic model

Database ID	Statistical parameter	F_o, N (lbs)	k_o, kN/m (lbs/in)	r_1	r_2	r_3	r_4	F_i, N (lbs)	Δ_{unl}, mm (in)	α	β
S-1	Median	2185.0 (491.2)	1839.6 (10,504.2)	0.020	−0.120	1.585	0.005	132.1 (29.7)	4.2 (0.166)	0.70	1.08
	SD	454.6 (102.2)	399.2 (2279.3)	0.000	0.055	0.161	0.000	1.3 (0.3)	0.4 (0.017)	0.01	0.11
S-2	Median	1499.9 (337.2)	3336.5 (19,051.7)	0.022	−0.055	1.418	0.005	258 (58.0)	4.4 (0.173)	0.71	1.20
	SD	413.2 (92.9)	110.7 (631.9)	0.003	0.134	0.151	0.000	19.1 (4.3)	0.3 (0.013)	0.02	0.29
S-3	Median	5224.0 (1174.4)	7824.0 (44,676.3)	0.020	−0.037	1.000	0.005	522.2 (117.4)	2.4 (0.093)	0.74	1.03
	SD	152.1 (34.2)	37.7 (215.4)	0.000	0.024	0.000	0.000	68.5 (15.4)	0.0 (0.001)	0.06	0.05
S-4	Median	3455.4 (776.8)	3852.5 (21,998.4)	0.032	−0.091	1.015	0.005	410.1 (92.2)	4.2 (0.167)	0.70	1.08
	SD	615.6 (138.4)	160.3 (915.5)	0.012	0.035	0.012	0.000	16.5 (3.7)	0.4 (0.016)	0.00	0.06
S-5	Median	5660.4 (1272.5)	13,928.1 (79,531.3)	0.020	−0.031	1.017	0.004	113.4 (25.5)	4.7 (0.184)	0.70	1.00
	SD	24.5 (5.5)	424.6 (2424.7)	0.000	0.016	0.023	0.000	0.9 (0.2)	0.0 (0.001)	0.00	0.00
S-6	Median	3900.6 (876.9)	9595.8 (54,793.3)	0.020	−0.020	1.000	0.003	278.9 (62.7)	2.7 (0.108)	0.70	1.00
	SD	275.8 (62.0)	333.9 (1906.8)	0.000	0.000	0.000	0.000	4.0 (0.9)	3.0 (0.012)	0.00	0.00
S-7	Median	4728.0 (1062.9)	8461.0 (48,313.6)	0.020	−0.021	1.204	0.004	52.0 (11.7)	3.9 (0.154)	0.70	1.00
	SD	347.9 (78.2)	412.0 (2352.6)	0.000	0.002	0.087	0.001	6.7 (1.5)	0.5 (0.018)	0.00	0.00
S-8	Median	4192.9 (942.6)	21,025.5 (120,058.7)	0.020	−0.020	1.002	0.003	105.0 (23.6)	2.5 (0.099)	0.70	1.00
	SD	611.2 (137.4)	812.1 (4637.3)	0.000	0.000	0.003	0.001	27.1 (6.1)	0.1 (0.005)	0.00	0.00
S-9	Median	4256.5 (956.9)	4189.5 (23,922.5)	0.020	−0.020	1.000	0.005	553.4 (124.4)	3.5 (0.136)	0.70	1.00
	SD	133.0 (29.9)	205.5 (1173.7)	0.000	0.000	0.000	0.000	8.5 (1.9)	0.4 (0.015)	0.00	0.00
S-10	Median	5741.3 (1290.7)	6849.6 (39,112.1)	0.020	−0.020	1.000	0.005	120.5 (27.1)	2.9 (0.116)	0.70	1.00
	SD	223.7 (50.3)	183.0 (1045.0)	0.000	0.000	0.000	0.000	3.1 (0.7)	0.4 (0.016)	0.08	0.33
S-11	Median	5707.1 (1283.0)	13,216.9 (75,470.6)	0.020	−0.020	1.000	0.004	690.8 (155.3)	2.5 (0.099)	0.70	1.00
	SD	1119.6 (251.7)	215.4 (1230.0)	0.038	0.005	0.000	0.001	290.5 (65.3)	0.3 (0.011)	0.00	0.00
S-12	Median	7580.2 (1704.1)	14,921.7 (85,205.0)	0.020	−0.021	1.000	0.004	403.5 (90.7)	2.5 (0.100)	0.70	1.00
	SD	209.5 (47.1)	577.0 (3294.8)	0.000	0.003	0.000	0.001	32.0 (7.2)	0.1 (0.004)	0.00	0.01
S-13	Median	6062.5 (1362.9)	3742.6 (21,371.0)	0.045	−0.228	1.059	0.005	3468.7 (779.8)	8.2 (0.323)	0.95	1.92
	SD	691.7 (155.5)	239.0 (1365.0)	0.035	0.194	0.019	0.001	173.5 (39.0)	3.0 (0.120)	0.07	0.12

Table 9 continued

Database ID	Statistical parameter	F_o, N (lbs)	k_o, kN/m (lbs/in)	r_1	r_2	r_3	r_4	F_i, N (lbs)	Δ_{unl}, mm (in)	α	β
S-14	Median	11,294.9 (2539.2)	26,743.6 (152,710.0)	0.150	−0.032	1.002	0.005	1694.3 (380.9)	0.5 (0.018)	0.93	1.82
	SD	N/A[a]	N/A[a]	N/A[a]	N/A[a]	N/A[a]	N/A[a]	N/A[a]	N/A[a]	N/A[a]	N/A[a]
S-15	Median	9120.2 (2050.3)	51,737.7 (295,429.8)	0.020	−0.145	1.000	0.001	820.7 (184.5)	1.6 (0.063)	0.88	1.47
	SD	3534.1 (794.5)	433.3 (2474.1)	0.000	0.092	0.000	0.000	341.2 (76.7)	0.1 (0.004)	0.02	0.31
S-16	Median	9987.1 (2245.2)	28,987.4 (165,522.2)	0.041	−0.027	1.000	0.005	998.6 (224.5)	5.1 (0.199)	0.93	1.80
	SD	N/A[a]	N/A[a]	N/A[a]	N/A[a]	N/A[a]	N/A[a]	N/A[a]	N/A[a]	N/A[a]	N/A[a]
S-17	Median	10,141.9 (2280.0)	(256,023.5)	0.157	−0.039	1.093	0.001	4474.0 (1005.8)	2.3 (0.089)	0.72	1.30
	SD	313.2 (70.4)	358.6 (2047.8)	0.115	0.000	0.132	0.002	117.9 (26.5)	0.000	0.00	0.00
S-18	Median	18,921.4 (4253.7)	74,863.0 (427,478.8)	0.020	−0.031	1.000	0.004	4557.6 (1024.6)	3.8 (0.148)	0.70	1.00
	SD	3071.9 (690.6)	447.1 (2552.8)	0.122	0.026	0.119	0.002	805.1 (181.0)	0.6 (0.022)	0.00	0.07
S-19	Median	10,008.9 (2250.1)	59,703.3 (340,914.8)	0.021	−0.045	1.000	0.005	5218.2 (1173.3)	1.8 (0.071)	0.732	1.207
	SD	2360.7 (530.7)	247.0 (1410.4)	0.001	0.022	0.601	0.002	564.5 (126.9)	0.5 (0.018)	0.128	0.404
S-20	Median	5560.7 (1250.1)	33,170.1 (189,406.1)	0.021	−0.045	1.000	0.005	2899.8 (651.9)	0.3 (0.012)	0.73	1.21
	SD	238.9 (53.7)	249.8 (1426.6)	0.001	0.022	0.601	0.002	56.9 (12.8)	0.000	0.13	0.40
S-21	Median	7784.8 (1750.1)	14,189.3 (81,023.1)	0.020	−0.052	1.000	0.008	1299.8 (292.2)	0.9 (0.037)	0.70	1.00
	SD	2572.0 (578.2)	366.3 (2091.6)	0.103	0.029	0.000	0.003	363.0 (81.6)	0.5 (0.018)	0.00	0.00
S-22	Median	9733.2 (2188.1)	14,738.3 (84,157.7)	0.261	−0.024	1.000	0.003	1361.2 (306.0)	1.2 (0.048)	0.86	1.65
	SD	1895.4 (426.1)	348.5 (1990.2)	0.275	0.009	0.109	0.003	546.2 (122.8)	0.2 (0.009)	0.12	0.43
S-23	Median	6733.7 (1513.8)	16,569.2 (94,612.5)	0.406	−0.041	1.000	0.001	1140.1 (256.3)	0.5 (0.019)	0.70	1.00
	SD	725.9 (163.2)	949.7 (5423.2)	0.272	0.018	0.012	0.000	399.5 (89.8)	0.1 (0.005)	0.11	0.41
S-24	Median	10,091.7 (2268.7)	42,721.5 (243,946.2)	0.099	−0.065	1.000	0.001	1576.8 (354.5)	0.5 (0.019)	0.70	1.00
	SD	693.0 (155.8)	392.5 (2241.4)	0.044	0.003	0.636	0.001	208.6 (46.9)	1.7 (0.065)	0.00	0.04
S-25	Median	10,510.3 (2362.8)	13,793.0 (78,760.1)	0.020	−0.060	1.000	0.002	1471.5 (330.8)	2.6 (0.101)	0.70	1.00
	SD	2664.0 (598.9)	228.9 (1306.8)	0.000	0.015	0.000	0.003	90.3 (20.3)	0.4 (0.014)	0.01	0.06

[a] Limited data sample to compute standard deviation

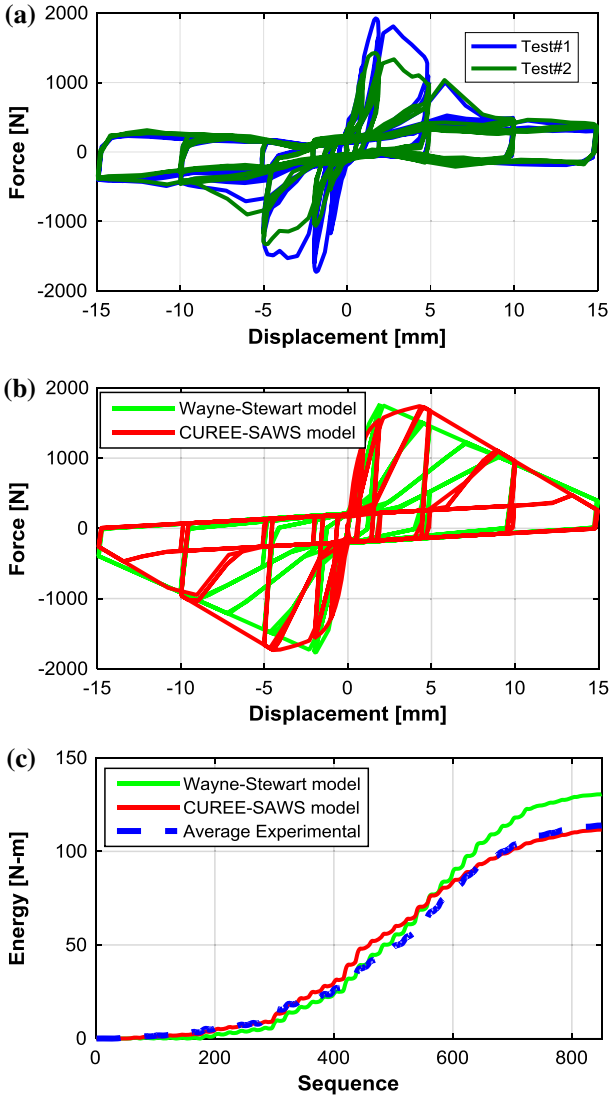

Fig. 7 Hysteretic response of button punches (20 ga) (S-2): **a** experimental results, **b** fitted–optimal hysteretic models and **c** energy absorption

designed per current design codes and standards in the United States (i.e. ASCE 7-10 and ACI 318-11). Details on the design of the low rise building can be found in Koliou (2014) and FEMA (2015).

A three step sub-structuring numerical framework was used for conducting nonlinear response analyses of the low rise building structure (Koliou et al. 2016a). The numerical framework incorporated the connector modeling using the diaphragm connector database as step 1 to be used in the numerical modeling of the roof diaphragm (step 2) and in the building model (step 3). An analytical roof diaphragm model was developed in step 2 incorporating the nonlinear response of the diaphragm connectors. This diaphragm model was validated with experimental data on a steel roof diaphragm available in the literature (Tremblay et al. 2004). Details on the validation study can be found in Koliou et al.

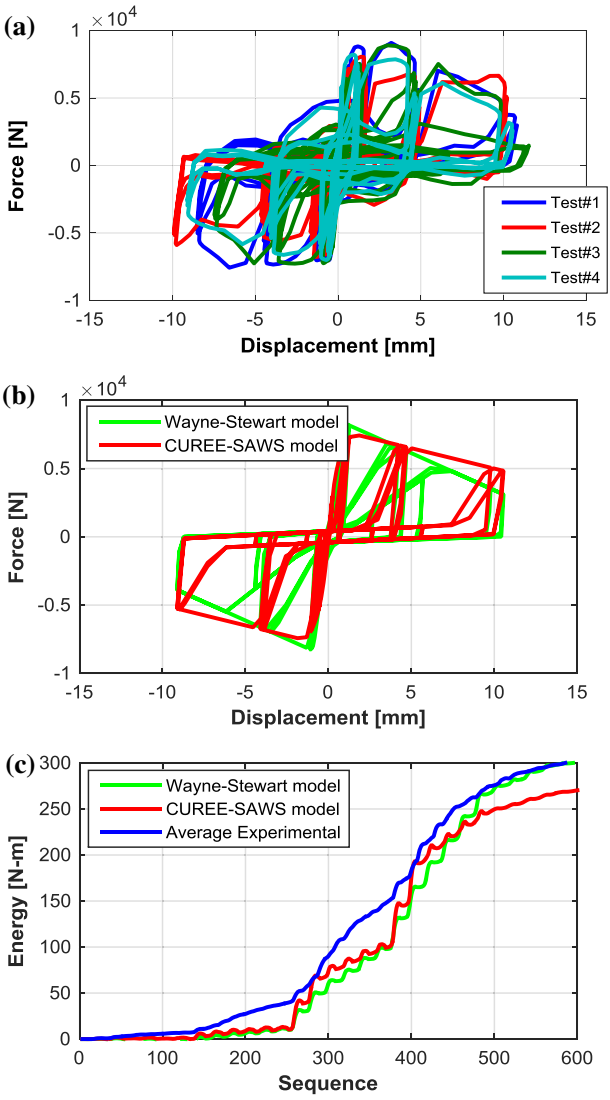

Fig. 8 Hysteretic response of PAFs (20 ga to a 201 mm plate) (S-9): **a** experimental results, **b** fitted–optimal hysteretic models and **c** energy absorption

(2016a). The building model of step 3 was used to perform IDAs under the FEMA P695 ground motion ensemble and evaluate the collapse performance of the low-rise building structure.

The spectral acceleration at the fundamental period of the building (computed $T_1 = 0.23$ s) was the IM considered, while the roof diaphragm drift ratio (*DDR*) (Cohen et al. 2004; Koliou et al. 2016b, 2017b), defined by Eq. (4), was considered as the EDP for this study. The *DDR* was selected as a representative EDP for this type of structure, which is dominated by the response of the flexible roof diaphragm compared to the rigid response of the in-plane walls. The sidesway collapse of the structure was considered as collapse

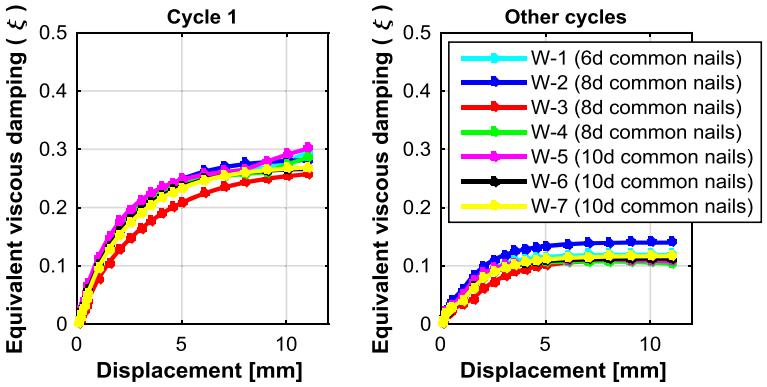

Fig. 9 Equivalent viscous damping ratio versus amplitude of cyclic loading of wood diaphragm connectors

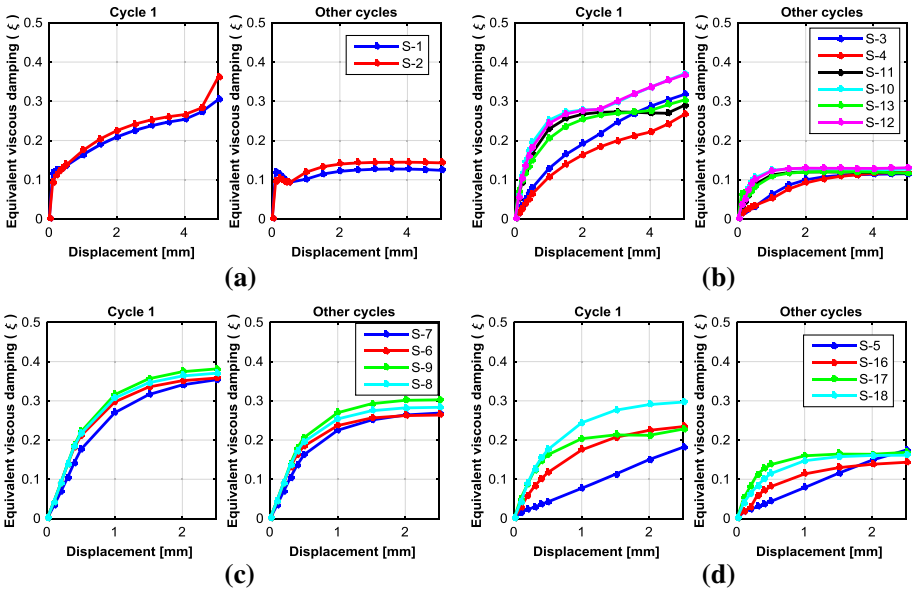

Fig. 10 Equivalent viscous damping ratio versus amplitude of cyclic loading of steel diaphragm connectors: **a** button punches, **b** screws, **c** PAFs and **d** welds

limit and was defined as the last survival intensity before the numerical building model becomes unstable accounting for P-Δ effects. A 2% of critical damping ratio was used for conducting non-linear time history analyses.

$$DDR = \frac{x_{mid,roof}}{\left(L_{roof}/2\right)} \tag{4}$$

where $x_{mid,roof}$ is the displacement at the center of the roof diaphragm, and L_{roof} is the horizontal span of the roof diaphragm.

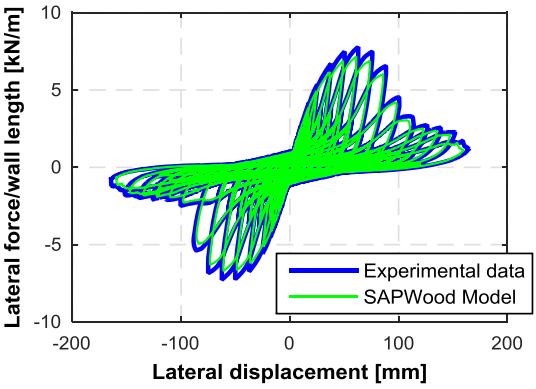

Fig. 11 Force–displacement response of light-frame wood wall system: comparison of experimental and numerical predictions

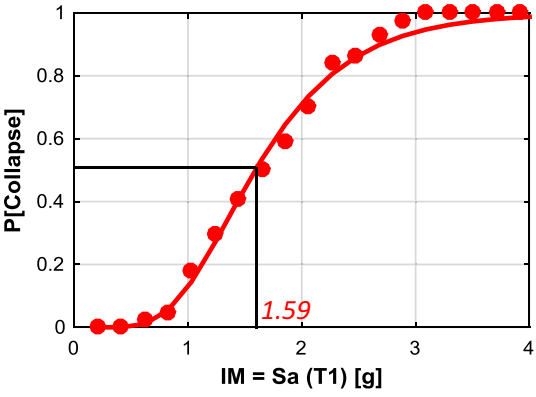

Fig. 12 Collapse fragility analysis results for light-frame wood wall system

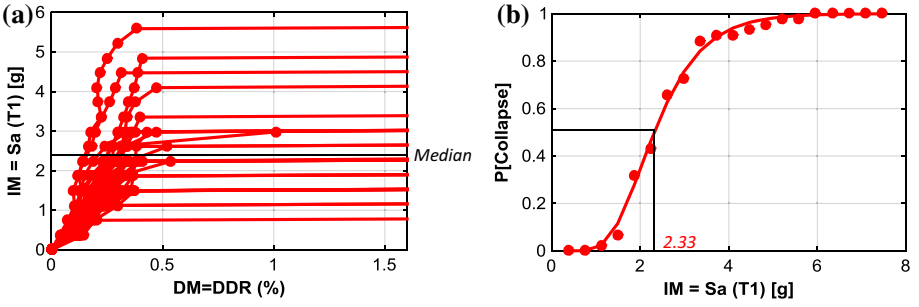

Fig. 13 Collapse analysis results for low rise building incorporating steel roof diaphragm: **a** IDA curves and **b** fragility curve

The IDA curves and corresponding collapse fragility curves are presented in Fig. 13a, b, respectively. A median collapse capacity of 2.33 g and standard deviation of 0.39, was found for the low-rise building structure incorporating a steel roof diaphragm.

The predicted collapse performance of the wood shear wall system and low-rise building with steel roof diaphragm, modeled considering the diaphragm connector database, incorporate the stiffness and strength degradation of the nonlinear connectors.

Reliable prediction of the collapse performance of components and systems cannot be achieved without incorporating experimentally obtained information on the modeling deterioration parameters of diaphragm connectors. The authors hope that the availability of the hysteretic parameter database for wood and steel diaphragm connectors developed in this paper will contribute to improved collapse assessments of these buildings.

5 Summary and conclusions

This paper focuses on the development and utilization of a steel and wood diaphragm hysteretic connector database for consideration into performance-based earthquake engineering (PBEE) studies. Accurate representation of structural members' stiffness and strength deterioration parameters are crucial into simulating components' and systems' dynamic response through collapse. To support accurate nonlinear modeling of wood and steel diaphragms, the hysteretic connector databases were developed. A wide range of experimental data for both wood and steel diaphragm connectors were considered to quantify the hysteretic parameters of the Wayne-Stewart and CUREE-SAWS hysteretic models considered into structural modeling. Wood diaphragm connectors included 6d, 8d and 10d common nails, while PAFs, screws, welds and button punches were used for the development of the steel diaphragm database. The statistical information of each connector type optimized hysteretic parameters (CUREE-SAWS and Wayne-Stewart models) are incorporated into the database. Furthermore, information on the energy dissipation properties of each connector type was identified in this study for possible consideration in Direct Displacement-Based Design (DDBD). A constant damping ratio at the range of 10–15% of critical was found for all common nails, button punches, screws and welds, while higher damping ratios of 25–30% of critical were identified for PAFs. The constant damping ratio values for various connector types could be beneficial into simplifying the DDBD for building structures incorporating wood and/or steel diaphragm systems.

The utilization of the developed diaphragm connector database in the context of the PBEE was demonstrated through two cases studies that assess their collapse capacity under certain seismic hazard. The first study investigated the collapse performance of a light-frame wood wall system, while the second one focused on the response of a low-rise building with a steel roof diaphragm.

Acknowledgements This study was partially conducted as part of work directed by the National Institute of Building Sciences (NIBS) and funded by the Federal Emergency Management Agency (FEMA) under DHS/FEMA Contract HSFEHQ-09-D-0147, Task Order HSFE60-12-J-0002C to develop simplified seismic design procedures for rigid wall-flexible roof diaphragm buildings. This financial support is gratefully acknowledged. The first author thanks the Structural Engineering and Earthquake Simulation Laboratory (SEESL) at the University at Buffalo for providing partial financial support. Any opinions, findings, and conclusions or recommendations expressed in this paper are those of the authors and do not necessarily reflect the views of the sponsors. Professors Robert Tremblay and Colin A. Rogers are also acknowledged for providing experimental data to support the steel diaphragm connector database.

References

Baber TT, Noori MN (1985) Random vibration of degrading, pinching systems. J Eng Mech 111(8):1010–1026

Bahmani P (2016) Personal communication

Bahmani P, van de Lindt JW (2014) Experimental and numerical assessment of woodframe sheathing layer combinations for use in strength-based and performance-based design. J Struct Eng 142(4):E4014001
Baker JW (2015) Efficient analytical fragility function fitting using dynamic structural analysis. Earthq Spectra 31(1):579–599
Barham W, Aref A, Dargush G (2005) Flexibility-based large increment method for analysis of elastic—perfectly plastic beam structures. Comput Struct 83(28):2453–2462
Berry M, Parrish M, Eberhard M (2004) PEER structural performance database user's manual (version 1.0). University of California, Berkeley
Ceccotti A, Vignioli A (1990) Engineered timber structures: an evaluation of their seismic behaviour. In: Proceedings of the international timber engineering conference. Science University of Tokyo
Chopra AK (2006) Dynamics of structures: theory and applications to earthquake engineering. Pearson Prentice Hall Upper Saddle River, NJ
Chou C (1987) Modeling of nonlinear stiffness and nonviscous damping in nailed joints between wood and plywood. Ph.D., Oregon State University, Oregon, p. 8724471
Christovasilis IP (2010) Numerical and experimental investigations of the seismic response of light-frame wood structures. Faculty of the Graduate School of the University at Buffalo, State University of New York, New York
Christovasilis IP (2011) Numerical and experimental investigations of the seismic response of light-frame wood structures. Ph.D., State University of New York at Buffalo, New York
Christovasilis IP, Filiatrault A, Wanitkorkul A (2009) Seismic testing of a full-scale two-story light-frame wood building: NEESWOOD benchmark test. Technical report MCEER-09-0005
Cohen GL, Klingner RE, Hayes JR, Sweeney SC (2004) Seismic evaluation of low-rise reinforced masonry buildings with flexible diaphragms: II. Analytical modeling. Earthq Spectra 20(3):803–824
Conte J, Zhang Y (2007) Performance based earthquake engineering: application to an actual bridge-foundation-ground system. In: Proceedings of the 12th Italian national conference on earthquake engineering, Pisa, Italy, pp 1–18
Cornell CA, Krawinkler H (2000) Progress and challenges in seismic performance assessment. PEER Center News 3(2):1–3
Coyne T (2007) UB-REU student project
Dean JA, Deam BL, Buchanan AH (1989) Earthquake resistance of timber structures. N Z J Timber Constr 5(2):12–16
Dolan JD (1989) The dynamic response of timber shear walls. Ph.D. dissertation, University of Bristish Columbia, Vancouver, British Columbia, Canada
Dolan JD, Gutshall ST, McLain TE (1995) Monotonic and cyclic tests to determine short-term load duration performance of nail and bolt connections volume I: summary report. Virginia Polytechnic Institute and State University Timber Engineering report no. TE-1994-001
Dowrick DJ (1986) Hysteresis loops for timber structures. Bull N Z Natl Soc Earthq Eng 19(2):143–152
FEMA (2009) Quantification of building seismic performance factors. FEMA P695, Federal Emergency Management Agency, Washington, DC
FEMA (2015) Seismic design of rigid wall-flexible diaphragm buildings: an alternate procedure. FEMA P1026, Federal Emergency Management Agency, Washington, DC
Filiatrault A, Christovasilis IP, Wanitkorkul A, van de Lindt JW (2009) Experimental seismic response of a full-scale light-frame wood building. J Struct Eng 136(3):246–254
Folz B, Filiatrault A (2001) Cyclic analysis of wood shear walls. J Struct Eng 127(4):433–441
Fonseca FS, Rose SK, Campbell SH (2002) Nail, wood screw, and staple fastener connections. CUREE publication no. W-16
Fülöp LA, Dubina D (2006) Design criteria for seam and sheeting-to-framing connections of cold-formed steel shear panels. J Struct Eng 132(4):582–590
Guenfoud N (2009) Shear and tension capacity of arc-spot weld connections for multi-overlap roof deck panels. École Polytechnique de Montréal
Huang X (2013) Diaphragm stiffness in wood-frame construction. University of British Columbia, Vancouver
Ibarra LF, Medina RA, Krawinkler H (2005) Hysteretic models that incorporate strength and stiffness deterioration. Earthq Eng Struct Dyn 34(12):1489–1511
Jin J, El-Tawil S (2003) Inelastic cyclic model for steel braces. J Eng Mech 129(5):548–557
Kivell BT, Moss PJ, Carr AJ (1981) Hysteretic modeling of moment resisting nailed timber joints. Bull N Z Natl Soc Earthq Eng 14:233–245
Koliou M (2014) Seismic analysis and design of rigid wall—flexible roof diaphragm structures. Ph.D., University at Buffalo, The State University of New York

Koliou M, Filiatrault A, Kelly DJ, Lawson J (2016a) Distributed yielding concept for improved seismic collapse performance of rigid wall-flexible diaphragm buildings. J Struct Eng 142(2):1–16
Koliou M, Filiatrault A, Kelly DJ, Lawson J (2016b) Buildings with rigid walls and flexible roof diaphragms. I: evaluation of current US seismic provisions. J Struct Eng 142(3):04015166
Koliou M, Filiatrault A, Kircher CA (2017a) Assessing modeling complexities on the seismic performance of an instrumented short-period hospital. J Perform Constr Facil 31(1):04016078
Koliou M, Masoomi H, van de Lindt JW (2017b) Performance assessment of tilt-up big-box buildings subjected to extreme hazards: tornadoes and earthquakes. ASCE J Perform Constr Facil. doi:10.1061/(ASCE)CF.1943-5509.0001059
Krishnan S (2010) Modified elastofiber element for steel slender column and brace modeling. J Struct Eng 136(11):1350–1366
LaBoube R, Sokol M (2002) Behavior of screw connections in residential construction. J Struct Eng 128(1):115–118
LaBoube RA, Yu W (1993) Behavior of arc spot weld connections in tension. J Struct Eng 119(7):2187–2198
Leach KE (1964) A survey of literature on the lateral resistance of nails. Department of Forestry (1085). Queen's Printer and Controller of Stationery, 12 p
Lignos DG, Krawinkler H (2012) Development and utilization of structural component databases for performance-based earthquake engineering. J Struct Eng 139(8):1382–1394
Lignos D, Karamanci E, Martin G (2012) A steel database for modeling post-buckling behavior and fracture of concentrically braced frames under earthquakes. In: Proceedings 15th world conference of earthquake engineering (15WCEE), September 24th–28th, Lisbon, Portugal
Lignos D, Karamanci E, Al-Shawwa N (2013) Structural component databases for performance-based earthquake engineering. In: 11th international conference on structural safety and reliability (ICOSSAR), New York City
Mack JJ (1961) The relation between nail withdrawal resistance and nail diameter and penetration. Division of Forest Products Technological Paper No 11. Commonwealth Scientific and Industrial Research Organization, Melbourne, Australia, 11 p
Mack JJ (1962) The strength of nailed timber joints. Division of Forest Products, C.S.I.R.O, Melbourne
MATLAB (2013) Version 8.10.1.604. The MathWorks Inc, Natick, Massachusetts
Moehle J, Deierlein GG (2004) A framework methodology for performance-based earthquake engineering. In: 13th world conference on earthquake engineering, pp 3812–3814
Mohammad MAH (1997) Stiffness responses of nailed OSB-to-lumber connections: influence of moisture conditioning and load cycling. Ph.D., The University of New Brunswick (Canada), Canada
Neuenhofer A, Filippou FC (1998) Geometrically nonlinear flexibility-based frame finite element. J Struct Eng 124(6):704–711
Ni C (1997) Behavior of nailed timber joints under reversed cyclic load. Doctor of philosophy, The University of New Brunswick, Canada
Otani S (1981) Hysteresis models of reinforced concrete for earthquake response analysis. J Fac Eng 36(2):125–159
Pei S, van de Lindt J (2010) User's manual for SAPWood for Windows: seismic analysis package for woodframe structures. NEEShub (nees. org)
Pekoz T (1990) Design of cold-formed steel screw connections. In: Proceedings of the 10th international specialty conference on cold-formed steel structures. University of Missouri-Rolla Rolla, St. Louis, pp 575–587
Pekoz T, McGuire W (1980) Welding of sheet steel. In: Proceedings, fifth international specialty conference on cold-formed steel structures, St. Louis, Missouri
Peuler M, Rogers C, Tremblay R (2002) Inelastic response of arc-spot welded deck-to-frame connections for steel roof deck diaphragms. In: Proceedings of the 16th international specialty conference on cold-formed steel structures, pp 763–778
Porter KA (2003) An overview of PEER's performance-based earthquake engineering methodology. In: Proceedings of ninth international conference on applications of statistics and probability in civil engineering
Rogers CA, Tremblay R (2003a) Inelastic seismic response of side lap fasteners for steel roof deck diaphragms. J Struct Eng 129(12):1637–1646
Rogers CA, Tremblay R (2003b) Inelastic seismic response of frame fasteners for steel roof deck diaphragms. J Struct Eng 129(12):1647–1657
Sideris P, Salehi M (2016) A gradient inelastic flexibility-based frame element formulation. ASCE J Eng Mech 142(7):04016039

Sivaselvan MV, Reinhorn AM (2000) Hysteretic models for deteriorating inelastic structures. J Eng Mech 126(6):633–640
Sivaselvan MV, Reinhorn AM (2006) Lagrangian approach to structural collapse simulation. J Eng Mech 132(8):795–805
Snow GL (2008) Strength of arc spot welds made in single and multiple steel sheets. Virginia Polytechnic Institute and State University, Blacksburg
Sokol MA, LaBoube RA, Yu W-W (1998) Determination of the tensile and shear strengths of screws and the effect of screw patterns on cold formed steel connections. University of Missouri, Rolla
Soltis LA, Mtenga PVA (1985) Strength of nailed wood joints subjected to dynamic load. For Prod J 35(11/12):14–18
Stewart WG (1987) The seismic design of plywood sheathed shear walls. Ph.D. dissertation, University of Canterbury, Christchurch, New Zealand
Tremblay R, Rogers CA (2005) Impact of capacity design provisions and period limitations on the seismic design of low-rise steel buildings. Steel Struct 5:1–22
Tremblay R, Martin E, Yang W, Rogers CA (2004) Analysis, testing and design of steel roof deck diaphragms for Ductile earthquake resistance. J Earthq Eng 8(5):775–816
Uriz P, Filippou FC, Mahin SA (2008) Model for cyclic inelastic buckling of steel braces. J Struct Eng 134(4):619–628
Vamvatsikos D, Cornell AC (2002) Incremental dynamic analysis. Earthq Eng Struct Dyn 31:491–514
Walter E (1995) Steel deck fasteners under low cycle fatigue. In: 5th US national conference on earthquake engineering, Chicago, IL, pp 827–836
Wilkinson TL (1976) Vibrational loading of mechanically fastened wood joints. Department of Agriculture, Forest Service, Forest Products Laboratory, Madison
Yarnell R, Pekoz T (1973) Test on field welded puddle and fillet weld connections. Cornell University, Department of Structural Engineering, Ithaca
Yuan Y-x (2000) A review of trust region algorithms for optimization. In: Ball JM, Hunt JCR (eds) ICM99: proceedings of the fourth international congress on industrial and applied mathematics. Oxford University Press, Oxford, pp 271–282
Zadanfarrokh F, Bryan E (1992) Testing and design of bolted connections in cold formed steel sections. In: Proceedings of eleventh international specialty conference on cold-formed steel structures